which is monoclinic, is ferromagnetic along the easy twofold b axis, but paramagnetic behavior was observed in all perpendicular directions.

Another crystal of large anisotropy is pyrrhotite, Fe_7S_8, first studied by Weiss[9] and later by Weiss and Foex.[10] In this hexagonal crystal the c axis is hard, but there is also considerable anisotropy in the basal plane. At room temperature the crystal is paramagnetic along the c axis, and ferromagnetic in the basal plane. Low-temperature studies are unfortunately not reported.

[9] P. Weiss, J. Phys. radium 4, 469 (1905).
[10] P. Weiss and G. Föex, *International Critical Tables* (McGraw-Hill Book Company, New York, 1939), Vol. 6, p. 366.

ACKNOWLEDGMENTS

The author is fortunate to have received valuable advice from Dr. A. Meckler, Dr. D. Greenberger, and Dr. A. Finn of the Department of Defense, and further wishes to thank T. Orlow, L. Bell, R. Gastrock, and A. Penn of the Naval Ordnance Laboratory Mathematics Department for computer programming.

PHYSICAL REVIEW VOLUME 124, NUMBER 5 DECEMBER 1, 1961

Galvanomagnetic Effects and the Band Structure of Antimony*

S. J. FREEDMAN AND H. J. JURETSCHKE
Polytechnic Institute of Brooklyn, Brooklyn, New York
(Received July 11, 1961)

The energy band structure of antimony is deduced from room temperature galvanomagnetic measurements and their interpretation in terms of a theoretical model. A systematic series of experiments is performed on oriented single crystals to measure all the 12 components of the isothermal resistivity tensor through second order in the magnetic field. The calculated galvanomagnetic effects assuming simple, independent three-valleyed bands for both the valence and conduction bands and isotropic relaxation times for both holes and electrons, are shown to fit the data by only one set of values for the 9 adjustable parameters in the theory. These parameters are: a set of three principal mobilities μ_i and ν_i, for electrons and holes, respectively; angles of tilt ψ_1 and ψ_2 of one of the principal axes of the electron and hole energy ellipsoids out of the base plane; and the carrier density N, the same for both carriers. The best fit is determined by exploring systematically a large number of possible solutions with the aid of an IBM 650 computer. If the "1" directions refer to binary symmetry axes and the "3" directions to those making angles ψ with the trigonal symmetry axis, the parameters have the values $\mu_1=0.15_4\times10^3$, $\mu_2=4.0_5\times10^3$, $\mu_3=1.1_8\times10^3$, $\nu_1=3.5_6\times10^3$, $\nu_2=3.3_0\times10^3$, $\nu_3=0.13_8\times10^3$ (all in cm²/volt-sec); $\psi_1=30.7°$, $\psi_2=63.2°$; $N=3.7_4\times10^{19}$ carriers/cm³ $=1.0_5\times10^{-3}$ carriers/atom. The results agree well with Shoenberg's de Haas-van Alphen data if the carriers responsible for the observed susceptibility oscillations are holes.

I. INTRODUCTION

THE general features of the electrical conduction processes in Sb have been known for some time.[1] They are attributed to a small though degenerate carrier population consisting of an equal number of both electrons and holes, with at least one of the overlapping bands multivalleyed. The energy surfaces of each valley are generally represented by ellipsoids tilted with respect to crystal axes.

The purpose of the present work has been to carry out a complete set of low-field room temperature galvanomagnetic (GM) measurements and to interpret these in terms of a general multivalley model for the bands. If the model is qualitatively correct, this procedure will determine the band structure. Partial interpretations of this nature have been worked out before on sets of data which were sufficient to specify only special multivalley structures. In this work the emphasis is on a systematic analysis of an overcomplete set of data permitting determination of all the nine parameters of a general multivalley model.

The presentation falls into three parts: (1) A series of experiments to determine all room temperature GM constants through second order in the magnetic field; (2) The calculation of GM effects for a model containing 9 adjustable parameters; (3) The adjustment of these parameters to obtain a best fit with experiment which then serves to specify quantities related to the band structure.

II. EXPERIMENTAL DESIGN

If the magnetic field dependence of the isothermal resistivity tensor can be expressed as a rapidly convergent series in powers of the field, a relatively small number of low-field measurements suffices to obtain all pertinent GM information for a finite parameter model. The number of independent coefficients appearing in the expansion depends on crystal symmetry, and the identification of these phenomenological constants in the Sb point group $\bar{3}m$, for transport processes characterized

* Supported by the Office of Naval Research. Part of a thesis submitted by S. J. Freedman in partial fulfillment of the requirements for the degree of Doctor of Philosophy at the Polytechnic Institute of Brooklyn.
[1] P. W. Bridgman, Proc. Am. Acad. Arts Sci. **63**, 351 (1929); K. Rausch, Ann. Physik **1**, 190 (1947); M. C. Steele, Phys. Rev. **99**, 1751 (1951); G. Busch and O. Vogt, Helv. Phys. Acta **27**, 241 (1954); C. T. Lane and W. A. Dodd, Phys. Rev. **60**, 895 (1941).

by a symmetric tensor,[2] shows that up to H^2 twelve constants are independent.

In this section we will describe the experimental arrangements of crystal orientations, currents, and fields actually used to obtain values for the room temperature, low-field GM constants.

The isothermal resistivity tensor in a magnetic field **H** is defined by

$$E_i=\rho_{ij}(\mathbf{H})J_j. \tag{1}$$

In a system of coordinates such that the crystallographic threefold axis (3) lies along z, and one of the crystallographic reflection planes contains the $y(2)$ axis, the components of ρ_{ij} for antimony, up to H^2, are

$$\begin{aligned}
\rho_{11}&=\rho_{11}{}^0+A_{11}H_1{}^2+A_{12}H_2{}^2+A_{13}H_3{}^2-2A_{24}H_2H_3,\\
\rho_{22}&=\rho_{11}{}^0+A_{12}H_1{}^2+A_{11}H_2{}^2+A_{13}H_3{}^2+2A_{24}H_2H_3,\\
\rho_{33}&=\rho_{33}{}^0+A_{31}H_1{}^2+A_{31}H_2{}^2+A_{33}H_3{}^2,\\
\rho_{23}&=R_{231}H_1-A_{42}H_1{}^2+A_{42}H_2{}^2+2A_{44}H_2H_3,\\
\rho_{31}&=R_{231}H_2+2A_{44}H_3H_1-2A_{42}H_1H_2,\\
\rho_{12}&=R_{123}H_3-2A_{24}H_3H_1-(A_{11}-A_{12})H_1H_2.
\end{aligned} \tag{2}$$

The remaining three components follow from the Onsager relations $\rho_{ij}(\mathbf{H})=\rho_{ji}(-\mathbf{H})$. These constants include the usual Hall and magnetoresistance (MR) effects. It is important to note, however, that the definition adopted in Eq. (1) for the coefficients of terms linear in H, yields constants R_{ijk} which are the negatives of the conventionally defined Hall constants.

To obtain measured values for these 12 phenomenologically independent constants it is necessary to perform experiments using a number of crystals with various orientations of **H** and **J** with respect to crystal axes. While the number of nonvanishing coefficients is relatively small, they make contributions to the measured voltages in a variety of experimental situations. This overlap makes it possible to connect measurements on different crystals and thus assures a consistent set of values for all constants.

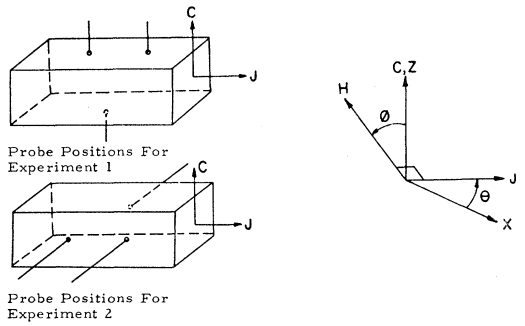

FIG. 1. Specification of the orientations of current and magnetic field with respect to sample in experiments 1, 2, and 3. Probe positions for experiment 3 are the same for 1 and 2 except that only two probes on one face are used. The angle θ is fixed; ϕ is varied at will.

[2] H. J. Juretschke, Acta Cryst. **8**, 716 (1955).

We list below the orientations and probe arrangements actually used, along with the phenomenological expressions for the electric field in each case. It is important to note that the expressions refer to polar axes fixed in the crystal with certain conventions for measuring angles. Since Sb is centro-symmetrical, the senses chosen for the polar z (threefold) and x (binary) axes can make no difference in the results. A consistent choice of x can be made by observing the secondary cleavage planes of Sb.

It is assumed that the samples are rectangular single-crystal rods of uniform cross section. The experimental arrangements below are grouped according to the direction of the current **J**.

A. $\mathbf{J}=(J\cos\theta, J\sin\theta, 0)$

(*a*) $\boldsymbol{H}\perp\boldsymbol{J}$. The sides of the crystal are chosen parallel and normal to the z axis. Three distinct experiments are performed on one crystal. The orientation of probes, currents, and fields for these three cases are given in Fig. 1.

Experiment 1 consists of a "Hall" measurement of the electric field in the z direction, E_z

$$1.\quad E_z=JHR_{231}\sin\phi+JH^2A_{42}\sin3\theta\sin^2\phi.$$

Experiment 2 consists of a "Hall" measurement of the electric field in the $\mathbf{z}\times\mathbf{J}$ direction, $E_{z\times J}$

$$2.\quad E_{z\times J}=-JHR_{123}\cos\phi+JH^2 2A_{24}\sin3\theta\sin\phi\cos\phi.$$

Experiment 3 consists of a resistivity and "transverse" measurement of the electric field along **J**, E_J

$$3.\quad E_J=\rho_{11}J+JH^2(A_{12}\sin^2\phi+A_{13}\cos^2\phi-2A_{24}\cos3\theta\sin\phi\cos\phi).$$

By a suitable choice of θ, all terms will eventually contribute.

(*b*) $\boldsymbol{H}\|\boldsymbol{J}$. An additional constant is obtained from the longitudinal voltage measured in experiment 4:

$$4.\quad E_J=\rho_{11}J+JH^2A_{11}.$$

If the crystal for this measurement differs from that used in (*a*), a connecting measurement is made by turning the sample 90° about the z axis, bringing it into a position corresponding to that of experiment (*a*)3. In this position,

$$5.\quad E_J=\rho_{11}J+JH^2A_{12}.$$

B. $\mathbf{J}=(0,0,J)$

There is no special orientation of the lateral faces in this case.

(*c*) $\boldsymbol{H}\perp\boldsymbol{J}$. A measurement of the longitudinal voltage E_J gives the new constants ρ_{33} and A_{31}:

$$6.\quad E_J=\rho_{33}J+JH^2A_{31}.$$

A measurement to connect these data consistently

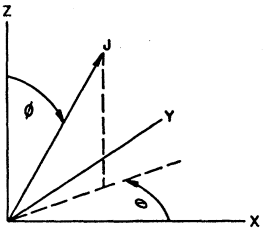

FIG. 2. Specification of the orientations of current and magnetic field with respect to crystal axes in experiments 10 and 11. The angles ϑ and ϕ are both fixed.

with those obtained in Sec. A is obtained from

$$7.\ E_{J\times H}=JHR_{231}-JH^2A_{42}\cos 3\theta.$$

Both constants appearing in this expression are also measured in A.

(*d*) $\boldsymbol{H}\|\boldsymbol{J}$. The longitudinal voltage of experiment 8 gives the new constant A_{33}.

$$8.\ E_J=\rho_{33}J+JH^2A_{33}.$$

A connecting measurement (experiment 9) with the crystal used for (*d*)8 placed in the position corresponding to (*c*)6 gives overlap on ρ_{33} and A_{31}.

C. H||J

The experiments outlined so far measure all constants except A_{44}. In order that A_{44} contribute at all to a longitudinal or transverse MR measurement, the crystal must be so oriented that **J** is parallel to **H** and makes an arbitrary angle with crystal axes. The convention for specifying orientations is given in Fig. 2.

The longitudinal voltage of experiment 10 contains A_{44}, and once this measurement is taken, A_{44} can be calculated from the previous results.

$$10.\ E_J=J(\rho_{11}\sin^2\phi+\rho_{33}\cos^2\phi)+JH^2[A_{11}\sin^4\phi+(A_{13}+A_{31}+4A_{44})\sin^2\phi\cos^2\phi+A_{33}\cos^4\phi].$$

A connecting measurement is taken by making **H** normal to **J**:

$$11.\ E_J=J(\rho_{11}\sin^2\phi+\rho_{33}\cos^2\phi)+JH^2(A_{12}\sin^2\phi+A_{31}\cos^2\phi).$$

The eleven measurements just described enable one to measure all the low-field GM constants in a consistent manner on several crystals. The expressions given apply on the assumption that the probes used are placed exactly along primary current flow lines. In practice there is always a small misalignment of the probes. Such misalignment produces spurious voltages and these contributions must be eliminated from the data before the GM constants can be obtained. Since it is possible to predict phenomenologically the H and angular dependence of these misalignment terms, they can be eliminated in all cases where necessary.

III. EXPERIMENTAL DETAILS

The samples used were rectangular parallelepipeds cut from large single crystals grown by the Bridgman method. Spectroscopic analysis of samples cut from the center of the crystals shows the purity to be about 99.994%.

Sb exhibits a number of prominent cleavages which can routinely be used to determine crystal orientation once the relation of cleavage planes to crystal axes has been determined. Back-reflection Laue photographs showed that the most prominent cleavages are perpendicular to *c*, the threefold axis. The traces of the secondary cleavages show threefold symmetry on the *c* faces and were shown by an oscillation photograph to be the directions of the binary axes by observing mirror symmetry perpendicular to the oscillation axis when this axis coincided with the secondary cleavage trace.

The samples were shaped by first cleaving along the *c* faces to obtain two parallel surfaces, and subsequently cutting with a diamond wheel while the crystal was under compression along the *c* axis. Care was taken to avoid undue strain, and samples so prepared gave consistent electrical properties. Heavy primary contacts were soldered to the ends of the crystal rods far enough apart to avoid any shorting effects.[3]

The secondary probes were made by welding No. 40 enameled copper wires onto the sample. Contact was made in a circular area of about 0.066-cm diameter. The distance between probes, usually about 0.5 cm, was measured with a microscope having a calibrated eyepiece.

The dc measurements were performed under isothermal conditions which were achieved by circulating a nonconducting fluid around the sample.

IV. EXPERIMENTAL RESULTS

Figure 3 is a plot of typical results obtained for the two "Hall" measurements in experiments 1 and 2 described in Sec. II. The transverse voltages are shown plotted against ϕ, the angle between *c* and H, for three

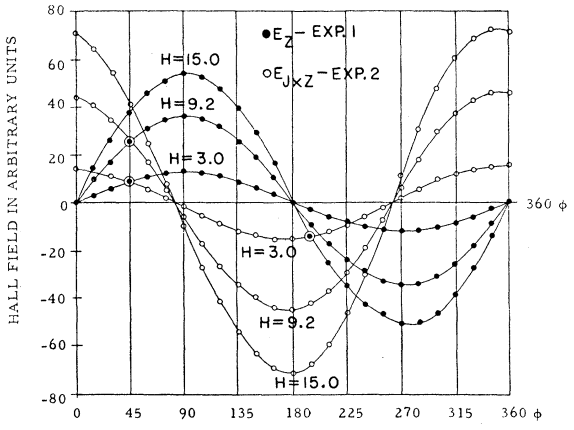

FIG. 3. Typical "Hall" data for experiments 1 and 2. H is given in kilogauss.

[3] J. Volger, Phys. Rev. **79**, 1023 (1950).

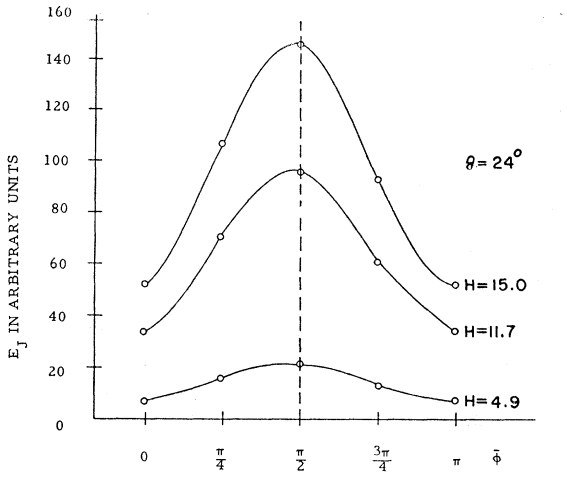

FIG. 4. Typical "magnetoresistivity" data for experiment 3 after averaging the data at ϕ and $\phi+\pi$ to eliminate misalignment.

values of H. The contributions of terms quadratic in H are apparent from the asymmetry about the zero volt line, while the contribution of cubic terms, not included in the expressions given in Sec. II, causes a shift in the extrema with H. Figure 4 shows typical results obtained for experiment 3 after the misalignment terms were eliminated by averaging the measurements at ϕ and $\phi+\pi$. The lack of symmetry about the dashed vertical line at $\pi/2$ is indicative of the presence of a contribution from A_{24}. Figure 5 shows the H dependence at constant ϕ of the averaged MR data of the previous figure. Here H^2/D, where D is the magnetoresistance, is plotted against H^2 yielding a straight line, the intercept of which is the inverse of the second-order constant A_{ij}, and the slope of which measures the contribution of the fourth-order constants. For the highest fields used, the effect of sixth-order constants is noticeable. No attempt

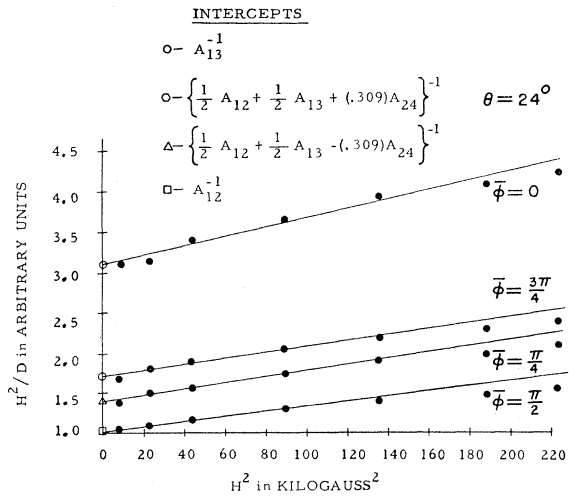

FIG. 5. Typical "magnetoresistivity" curves showing the magnetic field dependence at constant $\bar{\phi}$ of the data shown in Fig. 4. The inverses of the intercepts are measures of the second-order MR constants.

was made to analyze higher order terms since a systematic analysis would require large magnetic fields and a considerably greater number of crystal orientations.

Table I lists the final values obtained for all constants through second order. The numbers marked by an asterisk were obtained from Hall-type measurements while the unmarked ones are the results of MR-type measurements. For the particular choice of polar x axis used, both A_{24} and A_{42} are negative. The large value of ρ_{33} obtained for sample No. 33 is attributed to a crack in the crystal.

For the purpose of comparing experimental values with the calculations of the GM effects, discussed in Sec. V, it is desirable to evaluate the inverse constants characterizing the magnetic field induced changes in the conductivity tensor. The results of the inversion are given in Table II, along with the limits of error for each constant.

An examination of Table II will show that the conductivities σ_{ij}, and the inverse Hall constants $-P_{ijk}$, are almost isotropic, while there is a marked anisotropy in the magnetoconductivity (MC) constants. All constants compatible with crystal symmetry are nonvanishing, implying that the symmetry of conduction processes is not considerably higher than the structural symmetry.

V. GM EFFECTS IN THE NINE-PARAMETER MODEL

In this section we summarize the derivation of the form of the GM effects for the simplest model likely to lead to an explanation of the observed marked anisotropy.

If we assume that the bands are simple and that scattering can be described by a single relaxation time for the degenerate carriers, all observed anisotropies must be ascribed to the surfaces of constant energy composed of various oriented ellipsoids. Since all the MC constants are nonvanishing, the symmetry of the Fermi surface cannot be higher than $\bar{3}m$. We can obtain a structure having symmetry $\bar{3}m$ with a minimum number of extrema by placing one extremum in each of the three equivalent mirror planes of the point group and tilting the principal axes of the energy ellipsoids out of the base plane by a rotation about the binary axis. In this regard it is important to note that the point group $\bar{3}m$ will generate six extrema from a general point in the base plane lying in a mirror plane inside the zone. It is only when the extrema occur at the origin or at the center of the zone faces that three extrema obtain. For the case of independent extrema, i.e., no intervalley scattering, measurements of the GM effects do not enable one to decide among these cases. A six-ellipsoid model would change the results described in this section only by halving the number of carriers belonging to each extremum. The three-ellipsoid structure will be assumed for both electrons and holes. It contains, as a special case, the structure generally assumed for Bi, i.e., ellip-

TABLE I. Experimental values at 20°C for the components of the resistivity tensor in Sb. The asterisk indicates constants obtained from a "Hall" measurement.

	Resistivity: ρ_{ij} (10^{-6} ohm-cm)			Hall constant: $-R_{ijk}$ (10^{-7} ohm-cm/kgauss)		Magnetoresistivity constant: A_{ij} (10^{-9} ohm-cm/kgauss^2)								
Crystal	ρ_{11}	ρ_{33}	$\frac{1}{4}\rho_{11}+\frac{3}{4}\rho_{33}$	$-R_{231}$	$-R_{123}$	A_{11}	A_{12}	A_{13}	A_{31}	A_{33}	A_{44}	$-A_{42}$	$-A_{24}$	$\frac{1}{4}A_{12}+\frac{3}{4}A_{31}$
10	42.9			2.28*	2.50*		20.2	6.4				1.42*	3.5 3.5*	
13	43.1			2.15*	2.52*		19.6	6.4				1.3*	3.7 3.45*	
24	43.1					7.6		7.0						
50	42					7.1		5.9						
51									13.6					
32		36.3							13.6					
33		44.0							13.7	5.2				
41			40								−2.75			15.8

soids of revolution for the valence band and a multi-valleyed tilted scheme for the electrons.[4] Moreover, it is in qualitative agreement with Shoenberg's[5] interpretation of the de Haas-van Alphen effect in antimony.

The model contains nine adjustable parameters: a set of three principal electron mobilities μ_i, a set of three principal hole mobilities ν_i, one angle of tilt for each mobility ellipsoid type, and the carrier density N, the number of electrons and holes being equal for the pure material.

With the above assumptions, the contribution to the conductivity of all extrema is additive.[6] For each ellipsoid, in its own principal axis system, Ohm's law takes the form

$$J_i=\sigma_{ii}[\mathbf{E}+(1/nec)(\mathbf{J}\times\mathbf{H})]_i, \tag{3}$$

where $\sigma_{ii}=en\mu_i$, $en\nu_i$ for electrons and holes, respectively. Equation (1) can be solved explicitly for the current density in a given set of fields $\mathbf{E}$ and $\mathbf{H}$, and, once this is known for each ellipsoid, the observable current-voltage relation is obtained by reexpressing it in the crystal axis system and summing over the contributions of all ellipsoids. This procedure has been carried out in a number of ways,[7] with the following results:

$$\begin{aligned}
\sigma_{11}&=\tfrac{1}{2}eN[(\nu_1+\alpha_2^2\nu_2+\beta_2^2\nu_3)+(\mu_1+\alpha_1^2\mu_2+\beta_1^2\mu_3)],\\
\sigma_{33}&=eN[(\beta_2^2\nu_2+\alpha_2^2\nu_3)+(\beta_1^2\mu_2+\alpha_1^2\mu_3)],\\
-P_{231}&=(eN/2c)\{[\nu_2\nu_3+\nu_1(\beta_2^2\nu_2+\alpha_2^2\nu_3)]\\
&\qquad-[\mu_2\mu_3+\mu_1(\beta_1^2\mu_2+\alpha_1^2\mu_3)]\},\\
-P_{123}&=(eN/c)\{[\nu_1(\alpha_2^2\nu_2+\beta_2^2\nu_3)]\\
&\qquad-[\mu_1(\alpha_1^2\mu_2+\beta_1^2\mu_3)]\}.
\end{aligned} \tag{4}$$

The results for the MC constants are rather complicated and are best presented in the form of Table III. Each constant B_{ij} is formed by summing the products of the column heading with the corresponding entry in each row once for the electrons and once for the holes.

It is important to note the following definitions with respect to the above formulas:

$$\begin{aligned}
&\alpha_1=\cos\psi_1,\quad \beta_1=\sin\psi_1 \quad \text{for electrons,}\\
&\alpha_2=\cos\psi_2,\quad \beta_2=\sin\psi_2 \quad \text{for holes.}
\end{aligned} \tag{5}$$

Note that $N(=3n)$ is the total volume density of contributing carriers. ψ is the angle of tilt between the crystal threefold axis $\mathbf{z}$, and the principal axis 3 of the ellipsoid. ψ is considered positive in the direction $\mathbf{z}\times\mathbf{x}$. The algebraic sign in the inverse Hall constants has been exhibited explicitly so that all mobilities are considered positive. An examination of the results demonstrates the importance of determining the signs of B_{24} and B_{42} since these are the only constants to change sign under the operations:

$$\begin{aligned}
&\alpha_2\rightarrow\beta_2,\quad \beta_2\rightarrow\alpha_2,\quad \nu_1\rightarrow\nu_3,\quad \nu_3\rightarrow\nu_1;\\
&\alpha_1\rightarrow\beta_1,\quad \beta_1\rightarrow\alpha_1,\quad \mu_1\rightarrow\mu_3,\quad \mu_3\rightarrow\mu_1;
\end{aligned} \tag{6}$$

and are thus able to distinguish between models differing by this assignment. In contrast to the choice of

TABLE II. The magnetoconductivity constants.

Constants	Value computed from MR constants	Limits of error
σ_{11}	2.32×10^4 ohm^{-1} cm^{-1}	±2%
σ_{33}	2.75×10^4	±2%
$-P_{123}$	1.36×10^2 ohm^{-1} cm^{-1} kilogauss^{-1}	±3%
$-P_{231}$	1.44×10^2	±4%
B_{11}	4.0 ohm^{-1} cm^{-1} kilogauss^{-2}	±6%
B_{33}	3.9	±20%
$-B_{24}$	1.9	±6%
$-B_{42}$	0.87	±8%
B_{12}	11.5	±4%
B_{13}	4.2	±4%
B_{31}	11.2	±3%
$-B_{44}$	2.2	±20%

[4] B. Abeles and S. Meiboom, Phys. Rev. **101**, 544 (1956); G. E. Smith, *ibid.* **115**, 1561 (1959).

[5] D. Shoenberg, Proc. Roy. Soc. (London) **A245**, 1 (1952); Physica **19**, 791 (1953).

[6] Actually as shown by C. Herring and E. Vogt [Phys. Rev. **101**, 944 (1956)], this follows also for anisotropic relaxation times, as long as these are diagonal together with the energy surfaces.

[7] J. R. Drabble and R. Wolfe, Proc. Phys. Soc. (London) **B69**, 1101 (1956); J. R. Drabble, R. D. Groves, and R. Wolfe, *ibid.* **B71**, 430 (1958); T. Okada, J. Phys. Soc. Japan **12**, 1327 (1957); S. J. Freedman, Ph.D. thesis, Polytechnic Institute of Brooklyn (unpublished).

TABLE III. The calculated second-order magnetoconductivity constants. Each constant B_{ij} is formed by summing the products of the column heading with the corresponding entry in each row once for the electrons and once for the holes.

	$eN\mu_1^2\mu_2/c^2$	$eN\mu_1^2\mu_3/c^2$	$eN\mu_2^2\mu_1/c^2$	$eN\mu_2^2\mu_3/c^2$	$eN\mu_3^2\mu_1/c^2$	$eN\mu_3^2\mu_2/c^2$	$eN\mu_1\mu_2\mu_3/c^2$
$8B_{11}$	β^2	α^2	$3\alpha^2\beta^2$	α^2	$3\alpha^2\beta^2$	β^2	$-2-6\alpha^2\beta^2$
$8B_{12}$	$3\beta^2$	$3\alpha^2$	$\alpha^2\beta^2$	$3\alpha^2$	$\alpha^2\beta^2$	$3\beta^2$	$2-2\alpha^2\beta^2$
$2B_{13}$	α^2	β^2	α^4		β^4		$2\alpha^2\beta^2$
$-4B_{24}$	$-\alpha\beta$	$\alpha\beta$	$\alpha^3\beta$		$-\alpha\beta^3$		$\alpha\beta^3-\alpha^3\beta$
$-4B_{42}$			$-\alpha\beta^3$	$\alpha\beta$	$\alpha^3\beta$	$-\alpha\beta$	$\alpha\beta^3-\alpha^3\beta$
$-2B_{44}$			$\alpha^2\beta^2$		$\alpha^2\beta^2$		$\alpha^4+\beta^4$
$2B_{31}$			β^4	β^2	α^4	α^2	$2\alpha^2\beta^2$
B_{33}			$\alpha^2\beta^2$		$\alpha^2\beta^2$		$-2\alpha^2\beta^2$

sign of B_{24} and B_{42}, B_{44} is negative definite. That this is confirmed experimentally is encouraging.

Since 12 constants are calculated from a 9-parameter theory, the model predicts necessary relations among the constants. We have found two such for the general case of equal number of holes and electrons and arbitrary ellipsoid shape and orientation:

$$2B_{33}=(3B_{11}-B_{12}-2B_{44}), \tag{7}$$

and

$$4P_{231}[\sigma_{11}(-2B_{44})-\sigma_{33}B_{13}] =P_{123}[4\sigma_{11}B_{31}-\sigma_{33}(3B_{12}-B_{11}-2B_{44})]. \tag{8}$$

Both these relations are satisfied within experimental accuracy. The remaining relation was not found but is known to be of order higher than sixth in the mobilities.

The experimental data can also be tested against special model configurations. It is possible to rule out the case that holes alone contribute effectively to the GM effects, for in this case the following relation must obtain:

$$B_{31}/B_{13}=\sigma_{33}P_{231}/\sigma_{11}P_{123}. \tag{9}$$

Experimentally, the left- and right-hand sides of (9) are 2.67 and 1.25, respectively. The constants involved are among the most accurately known. For (9) to be satisfied, the experimental values must lie far outside the limits of error. We thus conclude that both carriers make a significant contribution to the GM effects.

Another special case can be ruled out immediately: that the angles of tilt for the surfaces belonging to both bands vanish. The resulting scheme has symmetry $\bar{6}m$. For this case the constants B_{33}, B_{24}, and B_{42} vanish identically. We therefore conclude that at least one set of ellipsoids is tilted.

VI. COMPUTATIONS. SPECIFICATION OF BAND STRUCTURE

In this section we will describe a method for searching rationally for the 9 parameters, if such exist, which when inserted into the expressions for the GM effects obtained in Sec. V, give agreement with the measured MC constants.

It was not found possible to solve directly for the parameters, partly due to the nature of the equations, and partly due to problems in distributing experimental errors. The Eqs. (4) and Table III were therefore recast into a form which would allow a systematic search for the best set of parameters.

Let us define measures of the electron and hole mobilities as follows:

$$\mu_1+\mu_2+\mu_3=fS; \quad \nu_1+\nu_2+\nu_3=(1-f)S, \quad \text{where} \quad S=(2\sigma_{11}+\sigma_{33})/eN. \tag{10}$$

Let us further introduce the dimensionless parameters

$$\begin{aligned} &x_1=\mu_1/fS; \quad y_1=\mu_2/fS; \quad z_1=\mu_3/fS;\\ &x_2=\nu_1/(1-f)S; \quad y_2=\nu_2/(1-f)S; \quad z_2=\nu_3/(1-f)S. \end{aligned} \tag{11}$$

With the above definitions, the physically meaningful range for the x's, y's, and z's lies between 0 and 1, since all mobilities must be positive and no single one alone is responsible for the total conductivity. It is also convenient to introduce reduced conductivities and inverse Hall constants.

$$\begin{aligned} &\Xi_1(1)=y_1+\alpha_1^2x_1+\beta_1^2z_1; \quad \Xi_3(1)=\beta_1^2x_1+\alpha_1^2z_1;\\ &\pi_1(1)=x_1z_1+y_1(\beta_1^2x_1+\alpha_1^2z_1); \quad \pi_3(1)=y_1(\alpha_1^2x_1+\beta_1^2z_1); \end{aligned} \tag{12}$$

with analogous expressions for quantities carrying the subscript 2. Note that $\Xi_1+\Xi_3=1$. It is now possible to write the following relations between experimentally observed ratios of numbers, and the unknowns N, f, and the reduced expressions of Eq. (12).

$$\begin{aligned} &f\Xi_1(1)+(1-f)\Xi_1(2)=2\sigma_{11}/(2\sigma_{11}+\sigma_{33})=S_1,\\ &f\Xi_3(1)+(1-f)\Xi_3(2)=\sigma_{33}/(2\sigma_{11}+\sigma_{33})=S_3,\\ &f^2\pi_1(1)-(1-f)^2\pi_1(2)=eNc\times 2P_{231}/(2\sigma_{11}+\sigma_{33})^2,\\ &f^2\pi_3(1)-(1-f)^2\pi_3(2)=eNc\times P_{123}/(2\sigma_{11}+\sigma_{33})^2,\\ &f^3\pi_3(1)\Xi_1(1)+(1-f)^3\pi_3(2)\Xi_1(2) =(eNc)^2 2B_{13}/(2\sigma_{11}+\sigma_{33})^3,\\ &f^3\pi_1(1)\Xi_3(1)+(1-f)^3\pi_1(2)\Xi_3(2) =(eNc)^2 2B_{31}/(2\sigma_{11}+\sigma_{33})^3,\\ &f^3\pi_3(1)\Xi_3(1)+(1-f)^3\pi_3(2)\Xi_3(2) =(eNc)^2(-2B_{44})/(2\sigma_{11}+\sigma_{33})^3,\\ &f^3\pi_1(1)\Xi_1(1)+(1-f)^3\pi_1(1)\Xi_1(2) =(eNc)^2(3B_{12}-B_{11}-2B_{44})/(2\sigma_{11}+\sigma_{33})^3. \end{aligned} \tag{13}$$

These eight equations are not independent. Because of Eq. (8), the last four equations contain one relation, and because $S_1+S_3=1$, the first two contain another. Thus, we have six equations for the eight independent unknowns N, f, and, say $\Xi_1(1)$, $\Xi_1(2)$, $\pi_1(1)$, $\pi_1(2)$, $\pi_3(1)$, $\pi_3(2)$. They fall conveniently into two groups, such that for given values of N and f we can consider Eq. (13) to define fully the reduced quantities of Eq. (12).

The application of the method is somewhat complicated because the relation of (8) is not satisfied exactly by the experimental data. However, by a least-squares distribution of errors, automatically stationary in f and N, it is possible to derive a consistent set of parameters for the right-hand side of Eq. (13), and therefore solve for the Ξ's and π's for given f and N.

Once the Ξ's and π's are known, all parameters introduced in (12) are determined:

$$\begin{aligned} y_l{}^u &= \tfrac{1}{2}\Xi_1[1\pm(1-4\pi_3/\Xi_1{}^2)^{\frac{1}{2}}], \\ x_l{}^u &= \tfrac{1}{2}(1-y_l{}^u) \\ &\quad\times\{1-[1-4(\pi_1-y_l{}^u\Xi_3)/(1-y_l{}^u)^2]^{\frac{1}{2}}\}, \\ z_l{}^u &= \tfrac{1}{2}(1-y_l{}^u) \\ &\quad\times\{1+[1-4(\pi_1-y_l{}^u\Xi_3)/(1-y_l{}^u)^2]^{\frac{1}{2}}\}, \\ (\alpha_l{}^u)^2 &= (\Xi_3-x_l{}^u)/(z_l{}^u-x_l{}^u). \end{aligned} \tag{14}$$

The indices u and l refer to solutions based on the upper or lower sign of the radical for y. The choice of sign before the radical of $z_l{}^u$ and $x_l{}^u$ corresponds to a particular choice of reference coordinates. With such choice we may require only that B_{24} and B_{42} have the proper relative signs.

The systematic fitting of the data then involves the following steps:

(1) Determination of the range of f and N leading to solutions of all the parameters in Eq. (14) lying between zero and unity. These are the conditions for positive mobilities and real angles of tilt.

(2) For a given f and N in this range, all MC constants can be computed and compared to experimental values; only those sets are retained for which B_{24} and B_{42} have the same sign, as found experimentally.

(3) Each acceptable solution is compared quantitatively to the experimental values by a least squares measure of over-all fit, and all solutions are classified accordingly.

The problem was run on an IBM 650 computer. For fixed input data (the experimental constants), the program sought solutions by varying f and N through ranges established by extensive hand and machine computations. The input was varied so that all combinations of the σ's and P's within experimental error were explored.

The search led to many real solutions. However, only one type of solution, characterized by parameters in a definite neighborhood, gave good agreement between experiment and all the computed constants. The values of the parameters for this solution are listed in Table IV and lead to the computed values of the MC constants as shown. The surprising, and gratifying, aspect of this result is, first of all, that the good solution is fairly unique, and furthermore, that it is reasonable. The density of carriers is in the anticipated range, the mobilities of electrons and holes are of similar and large magnitude and show pronounced anisotropy. Both sets of ellipsoids are tilted, and both contribute appreciably to observed effects, with the holes somewhat predominant. The assignment of angles of tilt was made according to the following prescriptions: In the experimental work, the polar direction of the threefold (**z**) axis was chosen so that **x**×**z** points down the slope of the secondary cleavage. With the convention adopted above for the positive direction of tilt, these definitions completely define the orientation of the mobility ellipsoids.

TABLE IV. Best values for the parameters appearing in the theory and comparison of experiment and theory using these parameters. The computed and measured conductivities and inverse Hall constants agree within 1%.

Carrier density $N=3.7_4\times10^{19}$ cm^{-3}								
Hole mobilities (10^3 cm^2/volt-sec)			Angle of tilt for holes		Electron mobilities (10^3 cm^2/volt-sec)			Angle of tilt for electrons
ν_1	ν_2	ν_3	ψ_2		μ_1	μ_2	μ_3	ψ_1
3.5_6	3.3_9	0.13_8	$63.2°$		0.15_4	4.0_5	1.1_8	$30.7°$
Constant		$8B_{11}$	$8B_{12}$	$2B_{13}$	$-4B_{24}$	$-4B_{42}$	$-2B_{44}$	$2B_{31}$	B_{33}
Theory		37.8	95.8	8.2_7	7.1_6	3.4_5	5.0_1	21.6	3.5_9
Experiment		32	92	8.5	7.6	3.5	4.4	22.4	3.9

Because of the closeness of the value obtained for the tilt of the electron mobility ellipsoids and the angle of one face of a Jones zone for Sb,[8] it is reasonable to assume tentatively that the electron overlap occurs on the (221)-type faces while holes are left on the $(1\bar{1}0)$ faces.

VII. DISCUSSION

The parameters listed in Table IV are the result of a systematic search for all possible physically acceptable fits of the model to the experimental data, and selecting the best set among these. We now discuss their numerical significance, the model upon which they are based, and the conclusions to which they lead.

Because of their interrelation in determining the parameters, it is very difficult to estimate how sensitive the results are to variation in the input data. Small changes can always be produced in this manner, but the experience of the program indicates that rather wide changes in the input data still lead to a "best" parameter set in the same neighborhood, defined by a given ordering in magnitude of the various principal mobilities and approximately constant angles of tilt. At least to this extent, and very likely to a rather more definite

[8] N. F. Mott and H. Jones, *The Theory of the Properties of Metals and Alloys* (Dover Publications, Inc., New York, 1958), p. 167.

TABLE V. Comparison of Shoenberg's de Haas-van Alphen data with the present results for holes. The isotropic hole relaxation time is taken to be $\tau_\nu = 1.1 \times 10^{-13}$ sec.

Parameter	Shoenberg	Present results
N (10^{-3} carriers/atom)	1.1	1.0_5
ν_1 (10^3 cm^2/volt-sec)	4.0	3.5_6
ν_2 (10^3 cm^2/volt-sec)	3.0	3.3_0
ν_3 (10^3 cm^2/volt-sec)	0.13_8	0.13_8
ψ	$55.2°$	$63.2°$

degree with respect to actual mobility anisotropies, the results reflect a basic connection between the experimental results and the model which is relatively insensitive to variations in detail of the former. Because the hole contributions to most measured constants predominate, most confidence should be placed in their parameters.

Of course, the model itself includes a number of more or less arbitrary assumptions. An essential part of the calculation of the GM constants is based on an isotropic relaxation time, so that the energy surfaces alone must account for the anisotropy in transport properties. For highly anisotropic energy surfaces, an argument due to Herring[9] suggests that this assumption is justified, since intravalley scattering can explore only one direction in reciprocal space regardless of the initial and final electronic states. The assumption of simple bands is an arbitrary one, but, once made, leads automatically to a multivalleyed model, as implied by nonvanishing B_{24} and B_{42}, and supported by the rather large value for a shear coefficient of piezoresistivity[10,11] $\frac{1}{2}(r_{14}+2r_{41})$ which would vanish if the energy surfaces are single ellipsoids of revolution. A multivalley structure has also been found necessary by Shoenberg[5] to explain the de Haas-van Alphen data. It is, of course, possible that all of these explanations really involve merely a multiple ellipsoid representation of a more complex band structure. In that case, experiments involving different averages should lead to different representations.

Shoenberg has been able to interpret the de Haas-van Alphen effects in Sb by assuming a single set of three energy surfaces tilted about the crystal binary axis, with inverse effective masses, expressed in a principal axis system, given by

$$m_0/m_{11}=20.0,\ m_0/m_{22}=0.68,\ m_0/m_{33}=15.4,\ \psi=34.8°, \quad (15)$$

and with a carrier density $N=1.1\times10^{-3}$ carrier/atom.

This density agrees fully with our results. If the relaxation time is isotropic, the inverse masses must be compared to our mobilities. Good agreement with our holes is, in fact, obtained if ν_2 and ν_3 are interchanged and if ψ_2 is replaced by its complement. This transformation corresponds to keeping the conventions in our theory fixed and letting $x \rightarrow -x$, $y \rightarrow -y$. We assume that Shoenberg's choice of either polar x or positive ψ was opposite to that of our theory. Combining the transformation $2 \rightarrow 3$, $3 \rightarrow 2$, $\psi \rightarrow \pi/2-\psi$ with an assumed hole relaxation time $\tau_\nu = 1.1\times10^{-13}$ sec, Shoenberg's data can be cast into a form comparable to ours, as exhibited in Table V. The agreement shown there is very good and indicates strongly that both types of experiment are consistent with the same model. It further implies that the Sb band structure remains basically fixed between liquid helium and room temperatures, and it also supports the isotropic relaxation time assumption. We conclude that the carriers responsible for the observed magnetic susceptibility oscillations appear to be holes.

Our results indicate that, under favorable conditions, a complete set of conductivity data can be analyzed systematically to lead to a fairly unique specification of band structure. Of course, such procedure will not be successful in all circumstances and even for antimony the assumptions which went into the model probably limit its applicability to the understanding of properties not too sensitive to band structure details. Nevertheless, the completeness of the specification of the band structure from relatively straightforward experiments to which the method leads makes it a natural guide for more detailed exploration.

ACKNOWLEDGMENTS

We wish to thank Dr. S. Epstein of the USASRDL, Solid State and Frequency Control Division, Fort Monmouth, New Jersey, who kindly supplied the single-crystal ingots and J. W. Mellichamp of the same laboratory who performed the spectroscopic analyses. We also wish to thank the staff of the Watson Scientific Computing Laboratory for providing the computing facilities used in this work.

[9] C. Herring, Bell System Tech. J. **34**, 237 (1955).
[10] M. Allen, Phys. Rev. **43**, 569 (1933).
[11] R. W. Keyes, Phys. Rev. **104**, 665 (1956).